УДК 532.012.2

HYDRODYNAMIC THEORY FOR A FLEXIBLE PROFILE VERTICAL AXIS TURBINE

D. ZEINER-GUNDERSEN

Norrent A.S., Slemmestad, Norway
Smiveien 19, 3470, Slemmestad, Norway
nor-a@online.no

Отримано 26.03.2014

Новая вертикальная осевая турбина с гибкими профилями была разработана и предварительно протестирована непосредственно в русле реки. Дизайн турбины базировался на предварительном упрощенном математическом анализе и тестировании модели для оптимизации взаимодействия турбины с окружающей гидродинамической средой. Проведена оценка нескольких аналитических моделей с точки зрения их сложности, точности и расчетного времени. Наиболее подходящей для дальнейших аналитических исследований и оптимизации конструкции гибкого профиля турбины признана каскадная модель. В данном случае оригинальная каскадная модель сочеталась с улучшенными эффектами динамического срыва, кривизны потока, изменением угла профиля. После таких улучшений настоящая модель становится сравнимой с теми, что используются для комплексного расчетного анализа динамики потока, но не требует значительных расчетного времени и расходов. Таким образом, модель, предложенная в данном исследовании, может быть использована для быстрой оценки экспериментов в лабораторных условиях и условиях эксплуатации, а также процесса оптимизации дизайна для улучшения функции и конструкции турбины в различных окружающих средах.

КЛЮЧЕВЫЕ СЛОВА: гибкий профиль турбины, гидродинамика, каскадная модель

Нова вертикальна осьова турбіна з гнучкими профілями була розроблена і попередньо протестована безпосередньо в руслі річки. Дизайн турбіни базувався на попередньому спрощеному математичному аналізі та тестуванні моделі для оптимізації взаємодії турбіни з навколишнім гідродинамічним середовищем. Проведена оцінка декількох аналітичних моделей з точки зору їх складності , точності та розрахункового часу. Найбільш відповідною для подальших аналітичних досліджень та оптимізації конструкції гнучкого профілю турбіни визнана каскадна модель. У даному випадку оригінальна каскадна модель поєднувалася з поліпшеними ефектами динамічного зриву, кривизни потоку, зміною кута профілю. Після таких поліпшень теперішня модель стає порівнянною з тими, що використовуються для комплексного розрахункового аналізу динаміки потоку, але не вимагає значних розрахункового часу і витрат. Таким чином, модель, що запропонована в даному дослідженні, можна використовувати для швидкої оцінки експериментів у лабораторних умовах і умовах експлуатації, а також процесу оптимізації дизайну для поліпшення функції і конструкції турбіни в різних навколишніх середовищах.

КЛЮЧОВІ СЛОВА: гнучкий профіль турбіни, гідродинаміка, каскадна модель

A novel vertical axis turbine with flexible profiles was designed and previously tested on-site in a river channel. The turbine design was based on initial simplified mathematical analyses and model testing done to optimize turbine interactions with the surrounding hydrodynamic environment. A study has been performed to evaluate several analytical models with respect to their complexity, accuracy, and computational time. The Cascade model was considered overall best suited for further analytical studies and optimizing the design of the flexible profile turbine. Herein, the original Cascade model was combined with improved dynamic stall effects, flow curvature effects, and profile pitching. After such improvements, the current model becomes comparable with those used for complex computational fluid dynamic analysis, but does not require significant computational time and expense. Hence, the model proposed in this study can be used for rapid assessment of field- and lab-based experiments and the design optimization process to improve turbine function and design in different environments.

KEY WORDS: flexible profile turbine, hydrodynamics, Cascade model

INTRODUCTION

A novel vertical axis turbine (herein named Pilot Z_{pilot}) was designed for hydrodynamic purposes. This Darrieus-inspired turbine used double cambered flexible profiles and passive pitching, with the design based on the dynamic thrust and flopping characteristics seen in aquatic creatures (Zeiner-Gundersen, unpublished). The flexible profile concept, together with pivot and spring arrangements, enabled dynamic profile movements, passive pitching, and limited variation in rotational speed versus incoming flow. On-site tests showed up to 37% turbine efficiency at optimal incoming flow speeds (Zeiner-Gundersen, unpublished). Optimization of the flexible profile turbine design depended on many factors, including knowledge of the interface interactions between the turbine and the surrounding environment. This paper describes a mathematical approach for analysis of the complex hydrodynamic fluid mechanisms in relation to the flexible turbine technology.

There are several 2-D and 3-D models applied to study the hydrodynamics of vertical axis turbi-

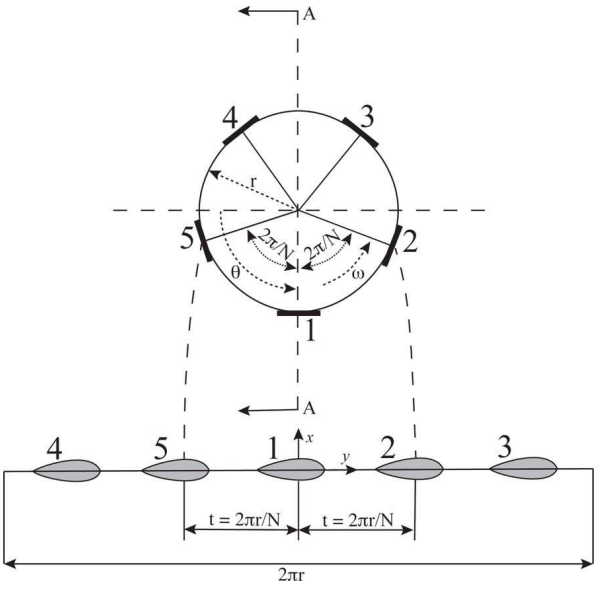

Рис. 1. Illustration of profiles (blades) in a cascade configuration

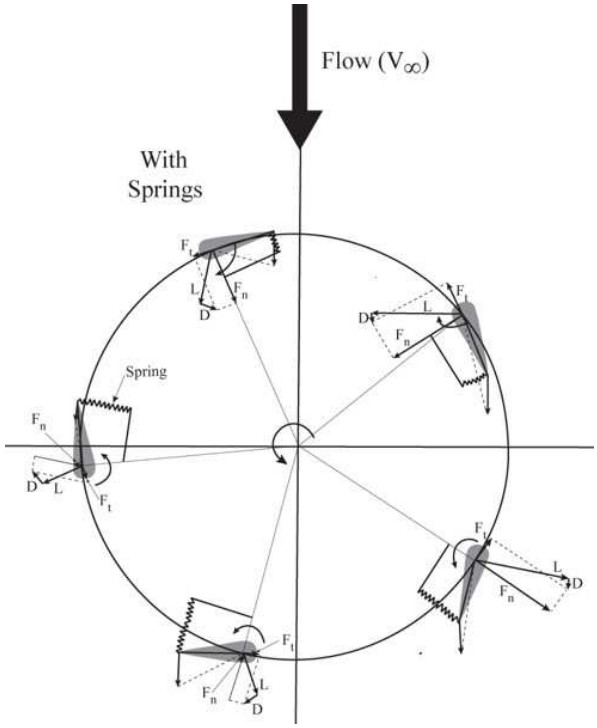

Рис. 2. Illustration of a turbine with five profiles showing a pitch arrangement and a passive rotational pivoting spring system, as is typical for the Pilot Z_{pilot} turbine

nes (e.g., [1-4]). The Cascade model was first applied for analysis of vertical Darrieus-type wind turbines by Hirsch and Mandal [5], and it has been widely used for the development of general turbine machinery for decades [6]. The Cascade model can be used for turbines with equidistant spacing of the blades/profiles/vanes in a planar position around the turbine circumference, in a so-called cascade configuration (Fig. 1). The hydrodynamic characteristics of each profile element are used for the upstream and downstream halves of the rotor, and incorporate the effect of the local Reynolds number variation at different azimuth angles (Fig. 2). Assuming that the first profile with an azimuth angle Θ is considered the reference profile 'one', the flow conditions of the 'second', 'third', and up to N profiles are assumed to be equal to those of the reference blade. To improve the analytical capability of the model, some dynamic stall and flow curvature factors were introduced by Mandal and Burton [7].

In this study, the Cascade model was further modified to predict the performance of the flexible profile vertical turbine. The present study combines the originally developed Cascade model with improved dynamic stall and flow curvature effects, as well as profile passive pitching. This study discusses the forces affecting the turbine in a free flow, including aspects such as general design parameters, fluid characteristics, the overall turbine dynamics, as well as flexible profile characteristics. After such improvements, the model becomes comparable to the more complex computational fluid dynamic analysis models, which in general require substantial modeling, computing time, and expense. In contrast, the modified Cascade model presented in this study can be used for more rapid assessment of parameters during the optimization of turbine design and performance in different environments.

1. BACKGROUND MATHEMATICAL BASIS FOR THE HYDRODYNAMIC ANALYSES

The turbine design process requires an iterative analytical approach that rapidly and efficiently determines the best compromise of various turbine parameters. Most computational models have the following key components:

1. Calculations of local relative velocities and attack angles at different tip speed ratios and azimuthal (orbital) positions.

2. Calculation of the ratio of induced free stream velocity considering the profile/profile-wake interaction.

3. Mathematical expressions based on either the Momentum, Vortex, or Cascade principles used to calculate normal and tangential forces.

4. The pre-stall wing profile characteristics for the configuration and attached regime at different Reynolds numbers.

5. Post-stall factor for continuous stall development and fully stalled regimes.

6. Tip speed and solidity ratio consideration.

7. Dynamic stall factor to account for the unsteady effects.

8. Flow curvature function to consider the circular motion of the wing profile.

All vertical axis turbines have their rotational axis perpendicular to the incoming flow. Most mathematical turbine models have been adapted to the wind industry, with low-density interacting fluid. In this study, certain parameters have been adjusted for the complex hydrodynamics of the flexible profile turbine. The general mathematical basis of these hydrodynamic analyses is described below.

1.1. Calculating energy inflow and extraction

The overall kinetic energy E is given by:

$$E = \frac{1}{2} m V_\infty^2, \tag{1}$$

where a fluid mass m flowing through a given area is given by

$$m = \rho A V_\infty. \tag{2}$$

By combining formulas, the energy in a free flow can be described by

$$P_0 = \frac{1}{2} \rho A V_\infty^3. \tag{3}$$

Thus, a certain amount of the inflowing energy in the free flow can be extracted, independent of the turbine design. This energy conservation method is given by the amount of fluid that must escape to let new fluid into the same area. The amount of energy that can extracted is given by

$$P = \frac{1}{2} C_p \rho A V_\infty^3. \tag{4}$$

In (1-4), C_p is the power coefficient of the turbine, is the fluid density, A is the cross-sectional area of the turbine, and V_∞ is the free flow velocity. P_0 is the available energy in a free flow, while P is the energy extraction by the turbine. Vertical axis turbines have a C_{pmax} of 64% (calculated using two actuator disks), which is based on the Betz theorem [8].

1.2. Factors affecting profile lift

The size of the forces affecting the thrust that drives profiles in a free flow depends on many parameters including the geometric configuration of the profiles, the angle of attack, flow velocity, the Reynolds number, and the Strouhal number (St; a dimensionless number describing oscillating flow mechanics). The most important profile parameters at any time are the radius of the leading edge, the curvature of the skeleton line, maximum thickness, distribution of the profile thickness, and the angle of the trailing edge.

Profile lift depends on the pressure distribution along the chord at the top and underside of the profile. Lift occurs according to the law of conservation of mass (whereby the mass of an isolated system will remain constant over time) and Newton's second law ($F = ma$; whereby F is the applied force, and m and a are the object's mass and acceleration, respectively). For a lifting profile, the pressure on the underside of the profile is greater than the upper side of the profile. The profile cambering effect versus lift and drag relative to the profile's angle of attack is also dependent on the flexibility within the profile. These data have been determined by extensive experimental testing in cavitation tunnels (data not shown). Furthermore, the use of Bernoulli's equation for incompressible flow in fluids, which is a representation of Newton's second law, demonstrates that (i) the speed of the upper side of a profile is faster than the bottom side when there is a lift, and (ii) both sides are equal at the trailing edge. The Bernoulli's equation is shown by

$$p = -\frac{1}{2} \rho W^2 - \rho g h + c. \tag{5}$$

The Bernoulli's equation therefore gives the dynamic pressure $1/2\rho W^2$, the hydrostatic pressure $\rho g h$, and the constant c. Bernoulli's equation is assumed to have constant, irrotational flow in a non-viscous fluid. For a profile immersed in a liquid, the hydrostatic pressure can be assumed to be almost zero regardless if it is horizontally or vertically mounted. Thus, the Bernoulli's equation without the hydrostatic pressure element only contains the variables for the pressure p and velocity W, with an increase in one or the other of the variables to maintain a constant c.

The lift and drag curves for the profiles are determined through testing and are used in the Cascade model. The measurements of lift, drag, momentum, and angle of attack for the original Pilot Z_{pilot} profiles were performed by SSPA at Chalmers University, Goteborg, Sweden in a cavitation tunnel on a set of scale models (data not shown). The double-cambered flexible profiles proved highly capable of handling large angles of attack and showed a good (slow) L/D linear decay versus angle of attack, which

would delay any profile stall and provide an improved general torque performance. This aspect is of particular importance for vertical axis turbines operating at low tip speed ratios with significant changes in the flow angle of attack versus the rotational azimuth angle.

The final design of a selected profile is also based on elements such as (i) high lift/drag ratios over a wide range of angle of attacks, (ii) sufficient mechanical strength for fatigue purposes, (iii) profile support that prevents local cavitation, (iv) double cambered functionality, (v) good static and dynamic stall characteristics, and (vi) a simple design. The material characteristics of the flexible elements should be flexible, have low coefficients of friction, and avoid unwanted marine growth on its surface.

1.3. Additional factors affecting turbine design and profile function

Several key parameters were considered when developing the flexible profile turbine, and are discussed herein.

A turbine's defined solidity σ is given by

$$\sigma = \frac{NC}{r}, \tag{6}$$

where N is the number of profile sets on the turbine, C is the chord length of the profile, and r is the turbine radius. The flexible profile turbine (Pilot Z_{pilot}) had a high solidity, with five profiles, giving it a robust design that helped reduce RPM variations.

The tip speed ratio (TSR; λ) is given by the ratio between the rotational speed at the leading edge of a profile and the relative flow of incoming water. The TSR is given by

$$\lambda = \frac{V_c}{V_\infty} = \frac{\omega r}{V}, \tag{7}$$

where ω is the rotational speed (rad/s), r is the turbine radius to the wing/arm tip (i.e. arm length), V_c is the actual relative speed of the profile, and $V_\infty$is the undisturbed incoming flow speed. Increased radius or increased rotational speed will lead to a higher TSR, as shown in (7).

In general, the Reynolds number Re is defined as

$$Re = \frac{\rho W L}{\mu} = \frac{WL}{\nu}. \tag{8}$$

The profile chord Reynolds number can be written as

$$Re = \frac{WC}{\nu}, \tag{9}$$

where W is the mean velocity of the object relative to the fluid, C is the profile chord length, ν is the kinematic viscosity ($\nu = \mu/\rho$), ρ is the density of the fluid, L is a characteristic linear dimension, and μ is the dynamic viscosity of the fluid. In contrast to the aerodynamics related to wing profiles, which have a $10^6 \div 10^8$ Reynolds number, a naturally moving free turbine has a characteristic $10^3 \div 10^6$ Reynolds number.

Herein, the author has defined a global turbine functionality parameter Z_s, reflecting the rotational behavior and the profile chord versus incoming water flow. Such parameters are generally used in the design and analytical process for describing occurrences taking place during rotation, such as foil pitching/flopping actions, foil-cambering transformations, rippling peaks affecting fatigue, and other significant occurrences related to performance. In particular, results from the test turbine Pilot Z_{pilot} showed a specific dominant foil flopping action for each of the five blades at 0° and 180° azimuth for each revolution, with each arm passing such a point and producing a local 'fishtail' foil flopping action (Fig. 3; further discussed in Zeiner-Gundersen, in preparation). As the blades, outfitted passive pivoting spring mechanism in the attachment point to the arm, rotated around the center axis, the foils were exposed to different relative flow angles of attack versus azimuth angles, resulting in different speeds relative to the angle of attack, thus creating the flopping motion of the foils as they rotated around the axis. This flopping motion helped to maintain a constant overall turbine RPM thus helping to mitigate the overall turbine fatigue. This flopping parameter resembles the definition of a Strouhal number. The parameter Z_s is defined as

$$Z_s = \frac{Ck_g}{V_{inf}}, \tag{10}$$

where V_{inf} is the fluid velocity flowing into the turbine, C is the profile chord length that is used as the characteristic length in the equation, and k_g is the turbine flopping frequency,

$$k_g = \frac{1}{T_g}. \tag{11}$$

The period T_g is assumed to be the dominant occurrence period such as for the Pilot Z_{pilot}. The dominant profile flopping motion, which for a turbine such as Pilot Z_{pilot} occurs five times per revolution ($\Theta_{arm-arm} = 72°$), can thus be written as

$$T_g = \frac{60s}{RPM} \cdot \frac{\Theta_{arm-arm}}{360°}. \tag{12}$$

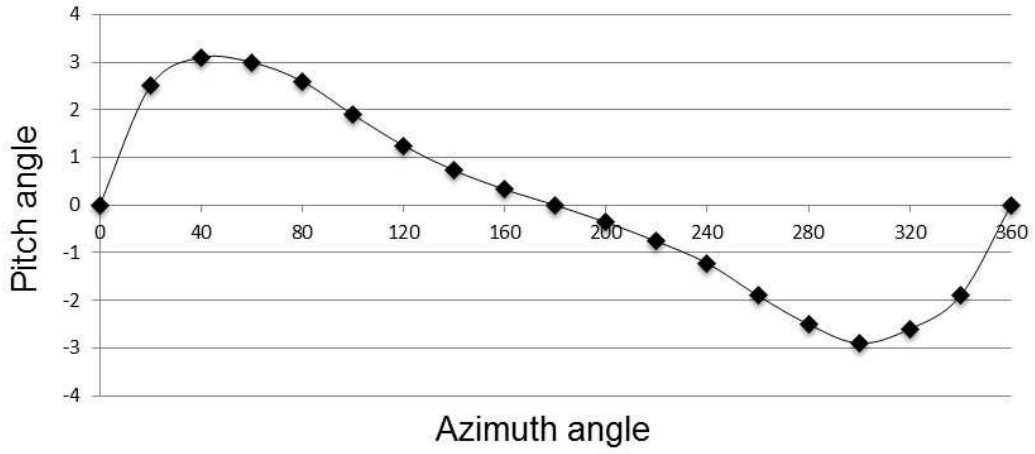

Рис. 3. Typical graph showing profile pitch angle for different azimuth angles, illustrating profile flopping actions. The diagram was estimated for 4.5 RPM, 1.4 m/s flow velocity, and 1.55 tip speed ratio

The Pilot Z_{pilot} turbine concept (Zeiner-Gundersen, unpublished) included a passive pivoting spring mechanism that enabled passive pitching of profiles depending on their position relative to the current flow, affecting their hydrodynamic behavior and improving turbine performance (Fig. 2). The hydrodynamic center of a profile is usually close to 25% of the chord length behind the leading edge. The dynamic pitching moment, herein M_n, is given by

$$M_n(\Theta) = \gamma(\Theta)k, \tag{13}$$

where γ is the pitching angle, and k is the rotational spring function around the profile pivoting point. Fig. 3 shows the changing pitch angle as a function of azimuth angle, and demonstrates the typical flopping motion of the profiles.

Field development and turbine design and function depend on many additional parameters: ocean, river, and tidal parameters such as water depth; number, spacing, and layout of installed turbines; "blockage area"and the hydrodynamic interactive effects between turbines; method of energy extraction (electric, pneumatic, or hydraulic) and energy transmission, and whether they are land- and/or ocean-based; structural fatigue of the turbine and profiles, which is also affected by the mechanical attachment methods between structural elements.

2. MODIFICATION OF THE CASCADE MODEL

The present study combines the originally developed Cascade model [5, 7] with further modifications based on overall turbine design, dynamic stall effects, flow curvature effects, and profile passive pitching. These modifications were essential for analysis of turbines with flexible profiles and passive pitching mechanisms.

2.1. Variation in the global attack angle

In general, the flow velocities cannot be considered as a constant for the upstream and downstream sides of a vertical style Darrieus-type turbine, in which the flow is considered to occur normal to the turbine axial direction (see Fig. 4 and 5). The chordal V_c and normal V_N velocity components, assuming no pitching, are given by

$$V_c = r\omega + V_a \cos\Theta, \tag{14}$$

$$V_n = V_a \sin\Theta, \tag{15}$$

where V_a is the induced flow velocity through the turbine rotor, ω is the rotational velocity, r is the turbine radius, Θ and is the azimuth angle assuming no pitching of the profile, as shown in Fig. 4. The angle of attack α is given by

$$\alpha = \mathrm{tg}^{-1}\left(\frac{V_n}{V_c}\right). \tag{16}$$

Substituting the values of V_n and V_c and non-dimensionalizing, the equation can be written without pitch angle as

$$\alpha = \mathrm{tg}^{-1}\left(\frac{\sin\Theta}{(r\omega/V_\infty)/(V_a/V_\infty) + \cos\Theta}\right), \tag{17}$$

where V_∞ is the free stream fluid velocity. Application of pivoting profiles as a function of the profile pitch

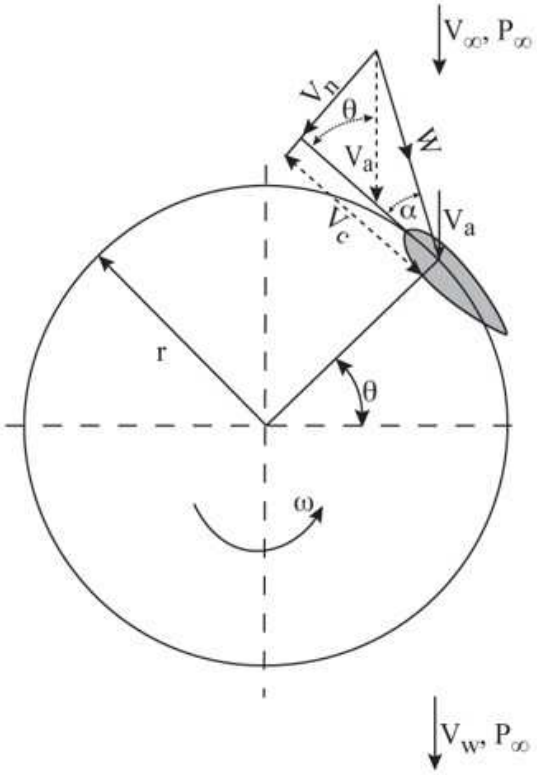

Рис. 4. Flow velocities defined for a vertical flex profile turbine

angle, $\gamma(\Theta)$, gives

$$\alpha = \mathrm{tg}^{-1}\left(\frac{\sin\Theta}{(r\omega/V_\infty)/(V_a/V_\infty)+\cos\Theta}\right) - \gamma(\Theta). \tag{18}$$

For the Pilot Z_{pilot} flexible profile turbine, the pivoting/pitching is a function of the rotational spring stiffness around the attachment point to the arm with a rotational linear spring factor k (compare to Fig. 4, which shows no pitching)

$$\gamma(\Theta) = M_n(\Theta)/k. \tag{19}$$

$M_n(\Theta)$ is the hydrodynamic profile's moment and is a function of the rotational azimuth angle and incoming speed V_{inf}, which is a function of the net moment-caused rotational effect of the lift and drag forces around the pivoting center of the profile for a turbine with active or passive pitching. The $M_n(\Theta)$, which is a function of the profile's azimuth position and incoming flow speed V_∞, can be extracted from the results of hydrodynamic testing of profiles for the Pilot Z_{pilot} (data not shown). The linear spring stiffness is a function of the selected design versus pitching as determined for the Pilot Z_{pilot} (data not shown).

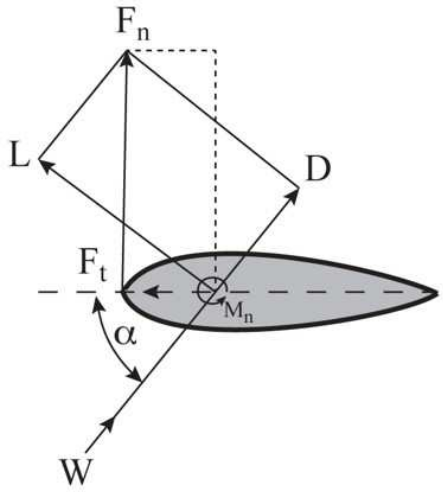

Рис. 5. Force diagram of a turbine profile

2.2. Variation of the local relative flow velocity

The relative flow velocity W is a function of velocity components, as in Fig. 4, and can be written as

$$W = \sqrt{V_c^2 + V_n^2}. \tag{20}$$

Inserting the values of V_c (14) and V_n (15) into (20), and non-dimensionalizing the equation by the velocity ratio, gives

$$\frac{W}{V_\infty} = \frac{W}{V_a}\frac{V_a}{V_\infty} = \sqrt{\left(\frac{r\omega}{V_\infty}/\frac{V_a}{V_\infty}+\cos\Theta\right)^2 + \sin^2\Theta}. \tag{21}$$

2.3. The variation in tangential and normal forces

The normal and tangential components of the lift and drag forces are shown in Fig. 5. The tangential C_t and normal C_n force coefficients are calculated by subtracting the corresponding coefficient of lift and drag forces, and this can be written as

$$C_t = C_l \sin\alpha - C_d \cos\alpha, \tag{22}$$

$$C_n = C_l \cos\alpha - C_d \sin\alpha. \tag{23}$$

The hydrodynamic profile's lift factor C_l and drag factor C_d are a function of the relative velocity W and angular α, which includes the pitch γ. The lift and drag are a function of the relative velocity and the net angle of attack.

The net tangential F_t and normal F_n forces on the profile at any specific moment can be written as

$$F_t = C_t \frac{1}{2}\rho C H W^2, \tag{24}$$

$$F_n = C_n \frac{1}{2} \rho C H W^2, \tag{25}$$

where ρ is the fluid density, C is the blade chord, and H is the turbine profile height.

2.4. Calculation of total torque and power output

The tangential and normal forces represented by (24) and (25) are for any azimuthal position and hence are a function of azimuth angle Θ. An average tangential force, F_{ta}, on one profile is calculated as

$$F_{ta} = \frac{1}{2\pi} \int_0^{2\pi} F_{ta}(\Theta) d\Theta. \tag{26}$$

The total torque Q for the number of profiles N can then be written as

$$Q = N F_{ta} r, \tag{27}$$

while the total power P can be calculated as

$$P = Q\omega. \tag{28}$$

2.5. Calculation of total torque and power output

As outlined above, the angle of attack on a profile (18) while the relative flow velocity can be written (21). This relative flow velocity can then be defined for the upstream as determined from Fig. 4 and 5. Fig. 6 shows the turbine profile velocity vectors for upstream (u) and downstream (d) positions.

Thus

$$\alpha_{ou} = \mathrm{tg}^{-1} \left(\frac{\sin\Theta}{(r\omega/V_\infty)/(V_{au}/V_\infty) + \cos\Theta} \right) - \gamma(\Theta) \tag{29}$$

and

$$\frac{W_{ou}}{V_\infty} = \frac{W}{V_{au}} \frac{V_{au}}{V_\infty} = \sqrt{\left(\frac{r\omega}{V_\infty} / \frac{V_{au}}{V_\infty} + \cos\Theta \right)^2 + \sin^2\Theta}\,. \tag{30}$$

The cascade configuration of the vertical flex profile turbine must be taken into consideration. The profile represented by '1' (see Fig. 1) at azimuth angle Θ is considered as the reference, and the other profiles represented by 2, 3, 4, and 5 are assumed to be equal to profile 1 (as is the case for the Pilot Z_{pilot} turbine). This process continues for one complete revolution of the reference profile 1 with profile steps $\delta\Theta$. Fig. 7 shows the velocity diagrams for a cascade profile. In order to execute the analysis, a control surface (stippled lines) is chosen, consisting of two lines parallel

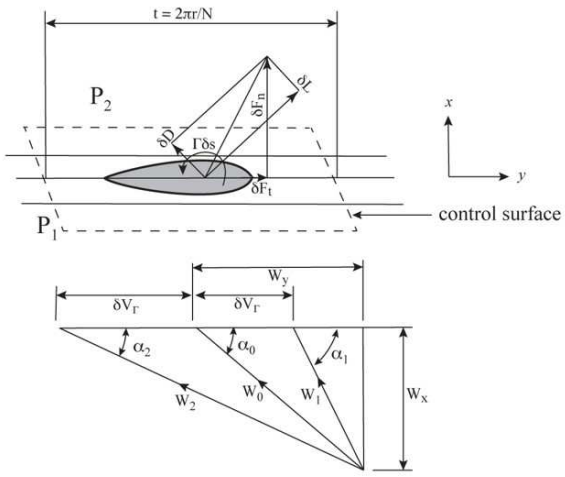

Рис. 7. Velocity diagrams for a Cascade model profile element

to the cascade plane and two identical streamlines having interspaces t.

The relative flow velocities W_1 and W_2 and corresponding angles of attack (α_1, α_2) at the cascade inlet and outlets can be determined from Fig. 7. The expressions are given by

$$\frac{W_1^2}{V_\infty^2} = \frac{W_x^2}{V_\infty^2} + \frac{(W_y - \delta V_\Gamma)^2}{V_\infty^2}, \tag{31}$$

$$\frac{W_2^2}{V_\infty^2} = \frac{W_x^2}{V_\infty^2} + \frac{(W_y + \delta V_\Gamma)^2}{V_\infty^2}, \tag{32}$$

$$\alpha_1 = \mathrm{tg}^{-1} \left(\frac{W_x/V_\infty}{(W_y - \delta V_\Gamma)V_\infty} \right) - \gamma(\Theta), \tag{33}$$

$$\alpha_2 = \mathrm{tg}^{-1} \left(\frac{W_x/V_\infty}{(W_y - \delta V_\Gamma)V_\infty} \right) + \gamma(\Theta), \tag{34}$$

where δV_Γ is the velocity contributed by the circulation $\Gamma\delta s$ (Γ is the circulation per unit length), and this is expressed as

$$\delta V_\Gamma = \frac{\Gamma\delta s}{2t} = \frac{N\Gamma\delta s}{2\pi r}. \tag{35}$$

2.6. Hydrodynamic forces in play

Fig. 7 shows that the pressure forces can be cancelled out along the bounding streamlines and the viscous forces can be eliminated outside the boundary layer surrounding the profile. Thus, only the momentum flux through the straight lines parallel to the cascade plane remains. The elemental force is in a tangential direction due to the relative rate of change of momentum as given by

$$\delta F_t = \delta m \left(W_2 \cos\alpha_2 - W_1 \cos\alpha_1 \right), \tag{36}$$

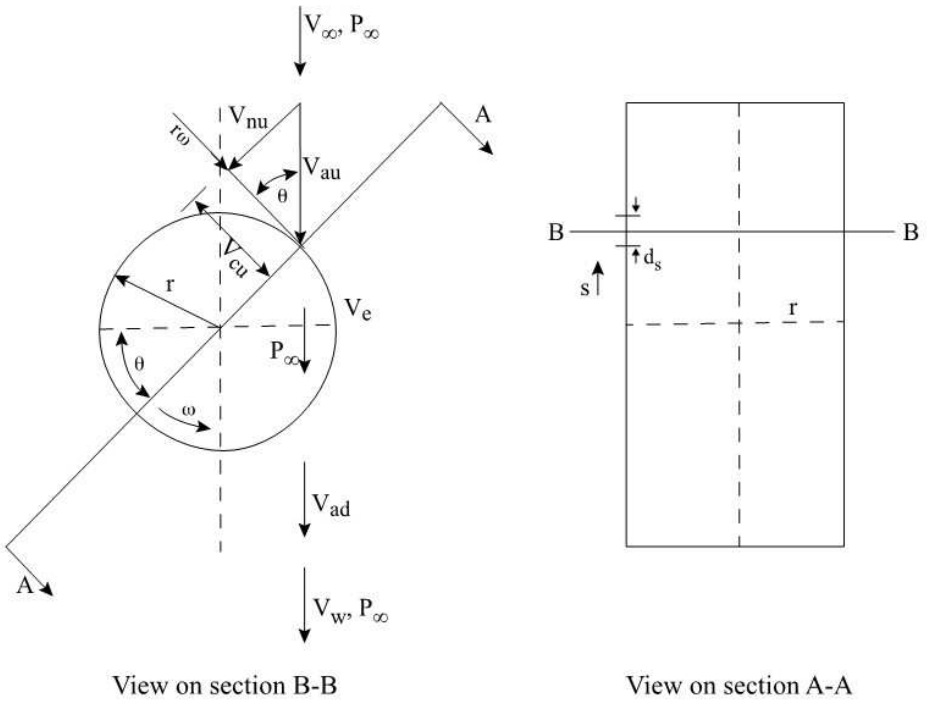

Рис. 6. A top view (left) and side view (right) of the turbine with vectorial velocities and notations denoting upstream (u) and downstream (d)

whereby $alpha_1$ and $alpha_2$ also include the pitching angle caused by the spring pivoting the profile. By applying the continuation equation, the elemental mass flow rate δm can be established as

$$\delta m = \rho t W_1 \sin\alpha_1 \delta s = \rho t W_2 \sin\alpha_2 \delta s = \rho t W_x \delta s, \tag{37}$$

while the elemental force in the normal direction to the defined cascade is given by

$$\delta F_n = \delta m \left(W_1 \sin\alpha_1 - W_2 \sin\alpha_2\right) + t(p_1 - p_2)\delta s\,. \tag{38}$$

Thus, by addressing the total cascade loss given by a total pressure loss term Δp_{0v}, and applying the Bernoulli's equation between the cascade inlet and the cascade outlet, gives

$$p_1 - p_2 = \frac{\rho}{2}(W_1^2 - W_2^2) + \Delta p_{0v}. \tag{39}$$

2.7. Velocity contribution as an effect of circulation

The velocity contributed by circulation around a profile is given by

$$\Gamma = \oint_s \overrightarrow{W}\overrightarrow{ds}. \tag{40}$$

The contribution along the parallel direction of the cascade plane is maintained. Thus the circulation becomes

$$\Gamma = t\left(W_2 \cos\alpha_2 - W_1 \cos\alpha_1\right). \tag{41}$$

From (36), (37), and (41), the tangential force can be written as

$$\delta F_t = \rho W_X \Gamma \delta s. \tag{42}$$

The elemental lift force (Fig. 8) can then be written as

$$\delta L = \delta L_{id} + \delta L_V, \tag{43}$$

where

$$\delta L_{id} = \delta F_t / \sin\alpha_0, \tag{44}$$

$$\delta L_V = \delta D / \mathrm{ctg}\,\alpha_0, \tag{45}$$

and $alpha_0$ is the angle of attack in rectangular flow (including the pitching). Thus, by introducing

$$\varepsilon = \delta D / \delta L, \tag{46}$$

into (42) and inserting

$$W_X = W_0 \sin\alpha_0, \tag{47}$$

the elemental lift force can be written as

$$\delta L = \rho W_0 \frac{\Gamma}{1 - \varepsilon \mathrm{ctg}\,\alpha_0}\delta s. \tag{48}$$

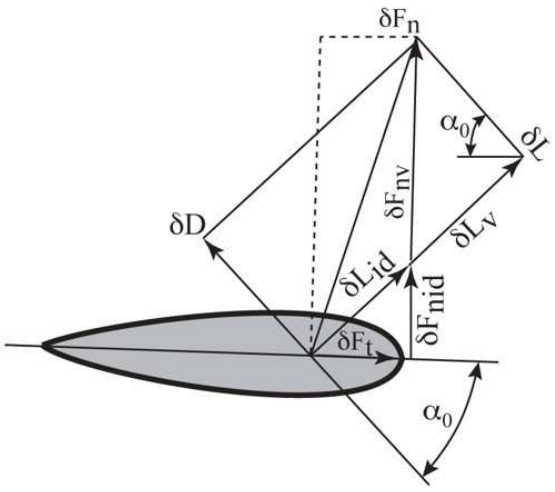

Рис. 8. Velocity diagrams for a Cascade model profile element

The elemental lift force is also defined as

$$\delta L = \frac{1}{2} C_l \rho W_0^2 C \delta s. \tag{49}$$

By determining the circulation from (48) and (49) and substituting in (40), the velocity contributed by the circulation is given by

$$\frac{\delta V_\Gamma}{V_\infty} = \frac{1}{8\pi} C_l \left(\frac{NC}{r}\right) \frac{W_0}{V_\infty} (1 - \varepsilon \operatorname{ctg} \alpha) \delta s. \tag{50}$$

2.8. Total pressure loss around the profile

The total pressure loss term can be determined using Fig. 8. The elemental normal force due to pressure loss can be obtained as

$$\delta F_{nv} = \delta D / \sin \alpha_0, \tag{51}$$

and the elemental force can then be written as

$$\delta F_{nv} = t \Delta p_{0v} \delta s, \tag{52}$$

while the element from the drag force δD can be defined as

$$\delta D = \frac{1}{2} C_d \rho W_0^2 C \delta s. \tag{53}$$

Thus, after introducing $t = 2\pi r/N$ and using (51) to (53), the equation for the pressure loss term can then be expressed as

$$\frac{\Delta p_{0v}}{\rho V_\infty^2} = \frac{1}{4\pi} \cdot \frac{C_d}{\sin \alpha_0} \left(\frac{NC}{r}\right) \frac{W_0^2}{V_\infty^2}. \tag{54}$$

2.9. Velocity ratios

By applying the Bernoulli's equation with the absolute velocities in front and behind the cascade gives the following equation

$$p_{1_u} - p_{2_u} = \frac{\rho}{2}(V_\infty^2 - V_e^2), \tag{55}$$

where V_e is the wake velocity and p_1 and p_2 are the pressure in front and behind the cascade element, respectively. Thus, by substituting the various parameters in (39) and (54) into (55), the relative wake velocity for the upstream side V_e can be written as

$$\frac{V_e}{V_\infty} = \sqrt{1 - \left(\frac{W_{2u}^2}{V_\infty^2} - \frac{W_{1u}^2}{V_\infty^2}\right) - \frac{1}{2\pi}\left(\frac{NC}{r}\right) \frac{C_{d_u}}{\sin \alpha_0} \frac{W_{0u}^2}{V_\infty^2}}, \tag{56}$$

while the relative wake velocity for the downstream side V_w can be written as

$$\frac{V_w}{V_e} = \sqrt{1 - \left(\frac{W_{2d}^2}{V_e^2} - \frac{W_{1d}^2}{V_e^2}\right) - \frac{1}{2\pi}\left(\frac{NC}{r}\right) \frac{C_{d_d}}{\sin \alpha_0} \frac{W_{0d}^2}{V_e^2}}. \tag{57}$$

Thus, in order to determine the induced velocity for use in further calculations, a relationship between the induced velocity V_a and the wake velocity (V_e, upstream; V_w, downstream) in the Cascade model can be defined for the upstream

$$\frac{V_{au}}{V_\infty} = \left(\frac{V_e}{V_\infty}\right)^{k_i} \tag{58}$$

and downstream

$$\frac{V_{ad}}{V_e} = \left(\frac{V_w}{V_e}\right)^{k_i}. \tag{59}$$

The value k_i is introduced as a factor that will compensate for (and be a function of) the turbine's solidity. Such a factor can be determined from experimental test results such as achieved for the turbine Pilot Z_{pilot} (data not shown). For new designs, such parameters could be determined and recommended based on model testing of a scaled turbine or interpolated from previous designs.

2.10. Dynamic stall

Dynamic stall is an important factor with a turbine that has profiles that will change angle of attack fairly rapidly. However, when the angle of attack α remains constant or varies slowly with time during the rotation, the turbine profiles will experience static stall. There are fundamental differences

between static and dynamic stall. The dynamic stall is an unsteady complex flow phenomenon and the hydrodynamic forces encountered from such dynamic stall will be much higher than for static stall. Thus, the Boeing-Vertol stall model [10] with modifications developed by Mandel and Burton [7] was applied to the Cascade model, with reference also given to [11] and the dynamics of vertical axis turbines [12].

A modified angle of attack that includes the pitch angle $\gamma(\Theta)$ was introduced and determined by the following factor

$$\alpha_m = \alpha' - \psi k_i \sqrt{\left|\frac{C\alpha'}{2W}\right|} S\alpha', \tag{60}$$

where α is the effective profile angle of attack, which includes the $\gamma(\Theta)$ angle, ψ and k_i are empirical constants, α represents the instantaneous rate of change of α, $S\alpha'$ is the sign of α', and W is the relative flow velocity. The modified angle of attack is thereby used to calculate the lift coefficient due to the dynamic stalling effect C_{ld} by

$$C_{ld} = \frac{\alpha}{\alpha_m} C_l(\alpha_m), \tag{61}$$

where $C_l(\alpha_m)$ is the lift value corresponding to the modified angle of attack, and α_m is extracted from two dimensional lift characteristics as tested in static stall conditions, such as could be valid for the hydrodynamic scale profile testing for the Pilot Z_{pilot} turbine.

Typically, for low Mach numbers and for an aerodynamic profile with > 0.1 profile thickness to chord ratio, the value of ψ is given by

$$\psi = 1.4 - 6(0.06 - t_c), \tag{62}$$

where t_c is the maximum profile thickness ratio. The k_i value will change with the sine of the effective angle of attack and is given by

$$k_i = 0.75 - 0.25(S\alpha'). \tag{63}$$

When the angle of attack is greater than the static angle or when it is decreasing after being above the stall angle, the modified Boeing-Vertol stall model was introduced. When the angle of attack is below the stall angle and/or increasing to the stall angle, the adjustment to the lift factor should not be incorporated into a model for computational purposes.

The dynamic C_{ld} is calculated by using the Boeing-Vertol model, and thus the lift coefficient in the pre-stall condition is obtained from the following relation

$$C_{lp} = P_f C_{ld}(\alpha_m) + (1 - P_f) C_l(\alpha), \tag{64}$$

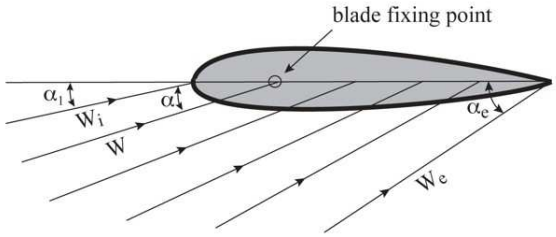

Рис. 9. Velocity diagrams for a Cascade model profile element

where P_f is a factor that is given by

$$P_f = (\alpha - \zeta)/(\alpha_s - \zeta), \tag{65}$$

α_s is the stall angle, and ζ) is the angular position from where the dynamic stalling effect is initiated up to where the profile stall angle is experienced.

In the analysis, the effect of drag characteristics due to dynamic stall use an empirical relation [10] defined as

$$C_{dd} = \frac{C_{ld}}{C_l(\alpha)} C_d(\alpha) K. \tag{66}$$

2.11. Effects of the profile flow curvature

The effect of the profile flow curvature can be applied as developed by Mandal and Burton [7] in the form of a simple analytical method, adjusting for the curvilinear nature of the flow. By applying this method, an adjustment can be made to the lift factor that is derived from tests, as in the case of the Pilot Z_{pilot} turbine. This factor is applied and corrected in consideration of the effect of dynamic stall. The effect is particularly important to include for high chord-radius ratio turbines and slow rotating turbines, which have significant continuous variation in flow velocity along the chord (see Fig. 9 for variations in flow angles along the profile). For the Pilot Z_{pilot} turbine, this effect was not significant due to the low chord to radius ratio and use of flexible profiles, although the turbine had slow rotational movement. Thus, the analysis should include this aspect.

The chord was assumed to be cambered in order to take into account the flow curvature effect, and thus the lift force was corrected while the relative flow velocity is preserved. The effect of the thin airfoil theory is introduced on an equivalent cambered hydrodynamic profile having a mean camber in the form of a circular arc, as also shown in Fig. 10. The equivalent cambered airfoil is found from the difference of the relative incident angle between the leading edge and the trailing edge by introducing

$$\beta = (\alpha_e - \alpha_i), \tag{67}$$

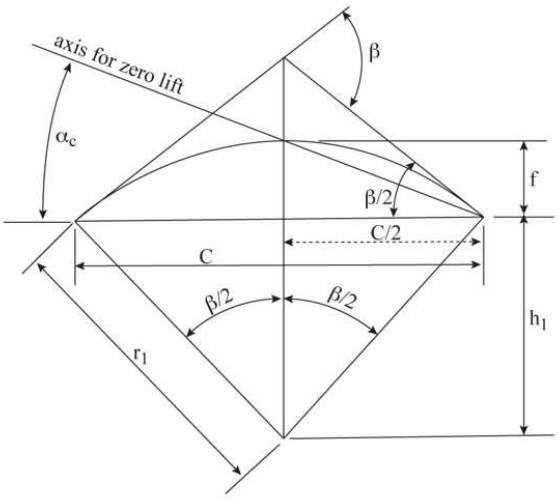

Рис. 10. Velocity diagrams for a Cascade model profile element

where α_i is the incident angle for the leading profile edge while α_e is the incident angle for the profile trailing edge.

From Fig. 10, the following can be calculated

$$r_l = \frac{C/2}{\sin \beta/2}, \tag{68}$$

$$h_l = \frac{C/2}{\operatorname{tg} \beta/2}, \tag{69}$$

where r_1 is the radius of the circular arc and h_1 is the maximum distance between the center and the chord of the circular arc. The maximum camber of the circular arc (f) is given by

$$f = r_l - h_l. \tag{70}$$

From (68) to (70), the following can be derived

$$\frac{2f}{C} = \frac{1 - \cos \beta/2}{\sin \beta/2}. \tag{71}$$

The incident correction angle is then given by

$$\alpha_c = \operatorname{tg}^{-1}\left(\frac{2f}{C}\right). \tag{72}$$

Combining (71) and (72) gives

$$\alpha_c = \operatorname{tg}^{-1}\left(\frac{1 - \cos \beta/2}{\sin \beta/2}\right). \tag{73}$$

Thus, in accordance with the thin 'airfoil' theory, the lift characteristics may be written as

$$C_{lc} = 2\pi \sin(\alpha + \alpha_c) \approx 2\pi(\alpha + \alpha_c). \tag{74}$$

The lift characteristic of a profile in accordance with thin aerofoil theory with zero chamber is then

$$C_l = 2\pi \sin \alpha \approx 2\pi\alpha. \tag{75}$$

Based on (74) and (75), the effect of the flow curvature will give correction to the lift factor, as defined by

$$F_f = C_{lc}/C_l = (\alpha + \alpha_c)/\alpha. \tag{76}$$

Thus, the initial static lift and drag should be corrected for the dynamic stall, so that the lift and drag functions are corrected for flow curvature.

Conclusions

Optimization of turbine design requires (i) iterative calculation, (ii) reflection of test data, and (iii) determining the effect of turbine solidity, pitching spring stiffness, hydrodynamic profile configuration, fatigue considerations, and field-specific conditions. For high solidity and lower speed tidal turbines such as the Pilot Z_{pilot}, the Cascade model must be carefully adjusted with respect to flow curvature effects, dynamic stall, the use of proper lift and drag curves, and profile flopping motions caused by energy release at specific azimuth angles versus analysis of hydrodynamic test data. Dai et al. [4] demonstrated that the Cascade model is a rapid computing model. This study improved the Cascade model to give comparable results as the more complex Vortex model. Hence, the present model provides an efficient and accurate interactive tool for optimizing the design and performance of a flexible profile vertical turbine under different environmental conditions.

1. *Urbina R., Peterson M. L., Kimball R. W., deBree G. S., Cameron M. P.* Modeling and validation of a cross flow turbine using free vortex model and a modified dynamic stall model // Renewable Energy.– 2013.– **50**.– P. 662–669.
2. *Li Y., Calisal S. M.* Three-dimensional effects and arm effects on modelling a vertical axis tidal current turbine // Renewable Energy.– 2010.– **35**.– P. 2325–2334.
3. *Goundar J. N., Ahmed M. R., Lee Y-H.* Numerical and experimental studies on hydrofoils for marine current turbines // Renewable Energy.– 2012.– **42**.– P. 173–179.
4. *Dai Y. M., Gardiner N., Sutton R., Dyson P. K.* Hydrodynamic analysis models for the design of Darrieus-type vertical-axis marine current turbines // Proceedings of the Institution of Mechanical Engineers, Part M: Journal of Engineering for the Maritime Environment.– 2011, **225**.– P. 295–307.
5. *Hirsch H., Mandal A. C.* A cascade theory for the aerodynamic performance of Darrieus wind turbines // Wind Engineering.– 1987.– **11**.– P. 164–175.

6. *Scholz N.* Aerodynamics of Cascades.– Neuilly-Sur-Seine, France: Advisory Group for Aerospace Research and Development, 1977.– 611 p.
7. *Mandal A. C., Burton J. D.* The effects of dynamic stall and flow curvature on the aerodynamics of Darrieus turbines applying the cascade model // Wind Engineering.– 1994.– **18**.– P. 267–282.
8. *Newman B. G.* Multiple actuator disc theory for wind turbines // Journal of Wind Engineering and Industrial Aerodynamics.– 1986.– **24**.– P. 215–225.
9. *von Ellenrider K. D., Parker K., Soria J.* Fluid mechanics of flapping wings // Experimental Thermal and Fluid Dynamics.– 2008.– **32(8)**.– P. 1578–1589.
10. *Gormont R. E.* A mathematical model of unsteady aerodynamics and radial flow for applications to helicopter rotors.– Philadelphia, Pennsylvania, U.S.A.: US AAMRDL Technical Report 72-67 for Boeing Company, 1973.– 138 p.
11. *Maniruzzaman M., Mandal A. C.* An investigation of the effect of dynamic stall on Darrieus turbines applying the cascade model // RERIC International Energy Journal AIT.– 1993.– **15(2)**.– P. 111–123.
12. *Abdel Azim El-Sayad A. F., Hirsch C., Derdelinckx R.* Dynamics of vertical axis wind turbines (Darrieus type) // International Journal of Rotary Machines.– 1995.– **2(1)**.– P. 33–341.